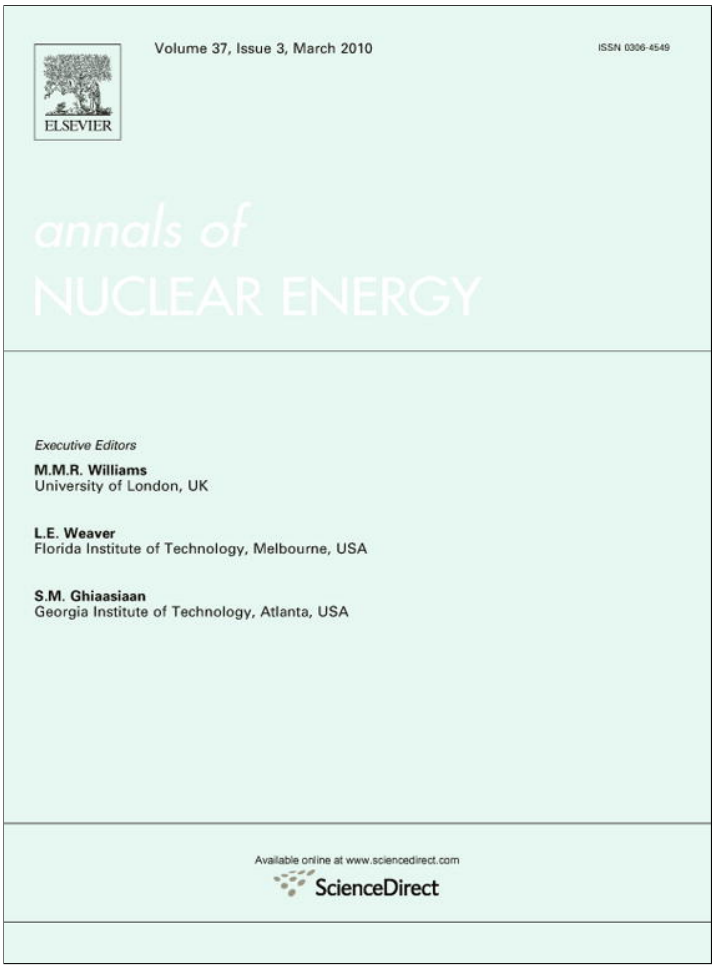

Annals of Nuclear Energy 37 (2010) 371–379

Contents lists available at ScienceDirect

Annals of Nuclear Energy

journal homepage: www.elsevier.com/locate/anucene

The effect of modern thermal neutron scattering sublibraries on criticality safety evaluations of wet storage pools

Edwin Kolbe *, Alexander Vasiliev, Hakim Ferroukhi

Laboratory for Reactor Physics and Systems Behaviour, Paul Scherrer Institut, CH 5232 Villigen PSI, Switzerland

ARTICLE INFO

Article history:
Received 16 July 2009
Received in revised form 27 November 2009
Accepted 3 December 2009
Available online 18 January 2010

ABSTRACT

Within the framework of a recent criticality safety evaluation (CSE) performed for the licensing of a new commercial wet storage pool using MCNPX-2.5.0 along with the ENDF/B-VII.0 and JEFF-3.1 continuous energy cross-section libraries, the maximum permissible initial fuel-enrichment limit for water reflected configurations was found to be dependant upon the applied neutron cross section library. More detailed investigations showed that the difference is mainly caused by different sublibraries for thermal neutron scattering based on parameterizations of the $S(\alpha, \beta)$ scattering matrix. This paper addresses the main findings of these investigations and emphasizes which configurations are particularly sensitive to the parameterization of $S(\alpha, \beta)$ applied in the CSE analysis. The results are presented in an attempt, on the one hand, to assess more precisely the sensitivity upon thermal scattering modeling data in CSE of wet storage pools, and on the other hand, to assess whether the data employed in the most recent neutron data libraries can be considered as an improvement for this type of analyses.

1. Introduction

A methodology for criticality safety evaluations based on MCNPX and continuous-energy data libraries has been developed at PSI (see Kolbe et al. (2008), and references therein). Recently, the methodology was applied for a CSE of a wet storage pool in a commercial Swiss nuclear power plant. In that context, the use of different cross-section libraries was found to yield consistent estimations of the maximum allowed fuel initial enrichment limit when analyzing the real storage pool configuration, while different results were obtained when considering a single fuel assembly immersed in water. Because the latter case was found to be the most limiting one in terms of the maximum allowed enrichment, it was considered necessary to further investigate the reason for the different behaviour between the two distinct neutron data libraries. The principal objective of this paper is to describe this study and to present the main findings that were obtained.

2. CSE methodology

2.1. Background

When two or more different calculational methods (CM, generally consisting of the computer code and the cross section data) are applied to determine the effective multiplication factor $\left(k_{eff}^{calc}\right)$ of a spent fuel system (SFS), the *absolute* values obtained for k_{eff}^{calc} with various methods will generally differ. However, the final results of a CSE of the SFS in terms of, e.g., the limits for the maximum permissible initial fuel-enrichment ($e^{\max}$) for fuel assemblies (FA) in a storage pool, should not significantly depend on the CM, because the generally different biases of CMs that lead to different absolute values of k_{eff}^{calc} should be properly accounted for in the upper subcriticality limit (USL) that enters the condition for subcriticality.

As a matter of principle, before a CM can be applied for the CSE of a SFS, its ability to accurately predict the subcriticality of such kind of systems must be demonstrated by performing a validation activity. Following Dean et al. (2001) a validation comprises the determination of the calculational bias (the systematic differences between calculational method results and experimental data) and its uncertainty by evaluation of a suite of critical experiments (benchmarks). The benchmark cases are selected according to the range of operating conditions and key physical parameters within which CSEs are expected to be performed in the future. This area of applicability must be outlined in the validation. Furthermore an analysis of trends should be performed, and, if trends are identified, they must be included in the definition of the USL. Finally all quantities established in the validation activity should be documented in sufficient detail in a formal report.

After validation a CM can be used to demonstrate the subcriticality of a specific SFS by calculating its effective multiplication factor k_{eff}^{calc} and verifying that the condition for subcriticality is fulfilled; e.g., this may be expressed by the relation:

$$k_{eff}^{calc} + \Delta k_{eff}^{calc} \leqslant \mathrm{USL}(x_s) = 1.0 + b(x_s) - \Delta b(x_s) - \Delta k_m \quad (1)$$

* Corresponding author. Tel.: +41 56 310 5155; fax: +41 56 310 2327.
E-mail address: Edwin.Kolbe@psi.ch (E. Kolbe).

0306-4549/$ - see front matter © 2009 Elsevier Ltd. All rights reserved.
doi:10.1016/j.anucene.2009.12.003

Here Δk_{eff}^{calc}, b, Δb, and Δk_m denote the uncertainty in the calculation of k_{eff}^{calc}, the bias, the uncertainty of the bias, and the administrative margin, respectively. The uncertainty in the calculational bias Δb includes the uncertainties in the cross section data and in the benchmarks, uncertainties due to limitations in the geometric or material representations of the benchmarks, and statistical and convergence uncertainties, or both, in the computation of the bias. If significant trends were found in the validation activity for one (or more) physical parameters x, the right hand side of Eq. (1) must be evaluated at the values x_s that these parameters take in the specific SFS. If no trends were found and a typical value of 0.05 is adopted for the administrative margin the condition for subcriticality reads:

$$k_{eff}^{calc} + \Delta k_{eff}^{calc} \leqslant \mathrm{USL} = 1.0 + b - \Delta b - 0.05 \tag{2}$$

One may note from this equation that absolute values of k_{eff}^{calc} determined by applying different CMs cannot be expected to agree, especially if the biases obtained from the validation of the CMs are strongly drifting. But the k_{eff}^{calc} corrected for the bias, i.e. the differences $k_{eff}^{calc} - b$, should lie close to each other (within Δb). Then all CMs should lead to similar results in terms of limits for physical parameters of the SFS (e.g., $e^{\max}$).

2.2. Calculational practice at PSI

A CSE methodology based on the international release version 2.5.0 of MCNPX (Pelowitz, 2005), published in April 2005, along with modern continuous energy neutron data libraries was recently established at PSI. Validation calculations were performed based on a suite of 15 low-enriched thermal compound uranium (LCT) and 4 mixed plutonium uranium thermal compound (MCT) benchmarks yielding a total of 149 critical experiments. All experiments were extracted from the "International Handbook of Evaluated Criticality Safety Benchmark Experiments" ("ICSBEP", OECD/NEA, 2005) and the selection of benchmark configurations was based on their similarity to designs found in today's LWR compact storage pools and transport casks. Details of the selection procedure and the characteristics of the benchmarks are described in (Vasiliev et al., 2005). In total five continuous energy cross-section libraries in ACE-format were assessed (Kolbe et al., 2008). Although significantly different biases were obtained with these CMs, the uncertainties of the biases in terms of the standard deviations of the normalized eigenvalues $k_{c,i} = k_{eff,i}^{calc} / k_{eff,i}^{bench}$ calculated for the validation suite were quite similar for all cross-section libraries. Furthermore, none of the libraries showed a trend when analyzing the full set of benchmarks. As the smallest biases were obtained with ENDF/BÙVII.0 (RSICC, 2007), and JEFFÙ3.1 (OECD/NEA, 2006), they both were selected as principal CMs in the PSI methodology. Moreover, in Sections 4 and 5 of this paper, ENDF/B-VI.8 (OECD/NEA, 2004) was applied (as provided by the NEA/OECD Data Bank) in order to perform a few comparison calculations.

3. Results for a Swiss wet storage pool

Recently, a CSE for a wet storage pool of a Swiss nuclear reactor was requested in the perspective of the introduction of a new fuel design. To that aim, the MCNPX-based methodology of Section 2.2 was applied using both ENDF/B-VII.0 and JEFF-3.1 libraries. In this CSE two configurations had to be considered:

(a) the entire storage pool and
(b) a single FA surrounded by an infinite water reflector.

For case (a), no deviating results between ENDF/B-VII.0 and JEFF-3.1 were found in terms of the $e^{\max}$ limit obtained by calculating the effective multiplication factors as a function of the fuel initial ^{235}U enrichment and applying Eq. (2). This is shown in the left-hand side of Fig. 1 where the effective multiplication factors calculated with ENDF/B-VII.0 (in red[1]) and JEFF-3.1 (in green) along with the Monte-Carlo errors are plotted. Note that in this figure, the dotted lines represent linear regression fits to the k_{eff}^{calc} obtained for a range of enrichments, while the horizontal solid lines represent the USLs derived with both libraries. This figure confirms that, as expected from the different biases obtained in the validation calculations, the absolute values for k_{eff}^{calc} are different, but the differences $k_{eff}^{calc} - b$ are in close agreement.

However, when analyzing case (b), non-negligible differences between both libraries emerged as illustrated in the right-hand part of Fig. 1. Here the intersection points of the dotted and solid lines define $e^{\max}$ with an uncertainty $\Delta e^{\max}$ accruing from the statistical uncertainties of the calculated eigenvalues and the uncertainty from the linear regression fit. Taking $\Delta e^{\max}$ into account one obtains the noticeably different enrichment limits denoted by $e^{\max}_{\text{E-VII.0}}$ and $e^{\max}_{\text{J-3.1}}$ in the figure. More precisely, noting that the distance between the USL-lines essentially reflects the differences in the bias between both libraries, it can be seen that it is not consistent with the distance between the linear regressions fits, resulting thereby in different limits for $e^{\max}$. More detailed investigations were therefore carried out and these have pointed out that the applied sublibraries for thermal neutron scattering could be one of the principal reasons for this unexpected behavior. This is described in the next section.

4. Study of thermal scattering effects on the benchmark suite

4.1. Basics of thermal neutron scattering

At neutron energies below about 4 eV the atomic binding of the scattering nucleus in a solid, liquid or gas has a non-negligible effect on the cross section and modifies the energy and angular distributions of the scattered neutrons. Following standard references (Parks et al., 1970; Squires, 1996) the double differential cross section for inelastic scattering of thermal neutrons can be written as:

$$\frac{d^2\sigma}{dEd\Omega}(E \to E', \mu) = \frac{\sigma_b}{4\pi kT}\sqrt{\frac{E'}{E}}e^{-\frac{\beta}{2}}S(\alpha,\beta) \tag{3}$$

where E and E' denote the energies of the incident and secondary neutron in the laboratory system, μ is the cosine of the scattering angle in the laboratory, σ_b is the bound scattering cross section for the material, kT is the thermal energy in eV, and $S(\alpha,\beta)$ is the symmetric form of the thermal scattering law. The scattering law is a function of only two variables, α and β, which represent (apart from constants) the momentum transfer:

$$\alpha = \frac{E' + E - 2\sqrt{E'E}\mu}{AkT} \tag{4}$$

and the energy transfer:

$$\beta = \frac{E' - E}{kT} \tag{5}$$

In Eq. (4) A denotes the ratio of the mass of the scattering atom to the neutron mass.

The cross section in Eq. (3) is related to the detailed dynamics of the atomic motion of the scatterer which usually is very complicated, i.e., hard to calculate. Nevertheless, approximations exist (Parks et al., 1970) to generate from (measured or calculated) frequency spectra of excitations (at a temperature T) the scattering

[1] For interpretation of colour in Figs. 1–8, the reader is referred to the web version of this article.

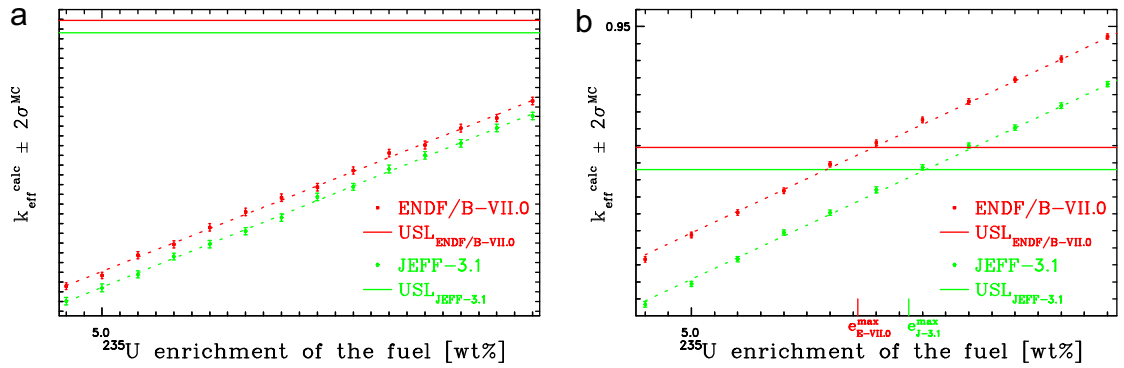

Fig. 1. Effective multiplication factors calculated with the JEFF-3.1 (green) and ENDF/BÙVII.0 (red) cross-section libraries as function of the ^{235}U enrichment for (a) the whole storage pool, and (b) a single PWR fuel assembly with an infinite water reflector.

law data files $S(\alpha, \beta, T)$ for a mesh of α and β values. In this way the LEAPR module (MacFarlane, 1994) of the NJOY code (MacFarlane and Muir, 1994) was used by Mattes and Keinert (2005) to (re)evaluate the thermal neutron scattering files for a range of materials including hydrogen bound in light water, and the resulting $S(\alpha, \beta)$ were found to reproduce the experimental data reasonably well (Mattes and Keinert, 2005). Note that, after extending the α and β grids to improve the energy region between 0.01 and 0.1 eV and after updating the physical constants to match the hydrogen and oxygen evaluations, the thermal neutron scattering sublibraries from Mattes and Keinert were included in the ENDF/B-VII.0 evaluated nuclear data file (Chadwick et al., 2006), and the new thermal neutron scattering kernel for H_2O was found to lead to a slight increase in the calculated k_{eff} eigenvalues for low-enriched thermal compound (LCT) critical assemblies(Chadwick et al., 2006).

With the ACER module of the NJOY code (MacFarlane and Muir, 1994) thermal scattering data in ACE format can be generated for use in the MCNP (MCNP, 2009) and MCNPX (MCNPX, 2009) codes.

4.2. Results and analysis

4.2.1. Effective multiplication factors for the benchmark suite

In Fig. 2 the values for k_{eff}^{calc} obtained by applying MCNPX-2.5.0 in combination with the ENDF/BÙVII.0 and JEFF-3.1 cross-section libraries are shown in comparison to the effective multiplication factors k_{eff}^{bench} evaluated in the 19 benchmark experiments including 149 cases. The 19 benchmarks are separated by vertical lines and are ordered by increasing benchmark and case number. With the numbers on the x-axis of Fig. 2 and the assignments listed in Table 1 each point in Fig. 2 can be attributed to the corresponding benchmark case. The uncertainties are represented by the error bars and match one standard deviation with respect to the calculations. By running 20 million active neutron histories, the MCNPX standard deviations σ^{MC} could be kept rather small (in the range of 10–20 pcm). As the confidence levels for the benchmark uncertainties σ^{bench} (the total uncertainty in k_{eff}^{bench}) is not specified for most of the ICSBEP evaluations, a value of one standard deviation was adopted (consistent with those cases in which the confidence level was explicitly stated).

Overall a very good agreement is found between the benchmark k_{eff}^{bench} values (shown in black) and the calculated eigenvalues. In most of the cases k_{eff}^{calc} (ENDF/B-VII.0) is slightly greater than k_{eff}^{calc} (JEFF-3.1). When only (i.e., all other cross sections of ENDF/B-VII.0 stay untouched) the $S(\alpha, \beta)$ for hydrogen in water from ENDF/B-VII.0 is replaced by the corresponding $S(\alpha, \beta)$ from JEFF-3.1, the MCNPX calculations lead to the multiplication factors shown in blue (denoted by ENDF/B-VII.0/$S(\alpha, \beta)_{J\text{-}3.1}$). For most of the benchmark cases this change of $S(\alpha, \beta)$ leads to a reduction of the calculated

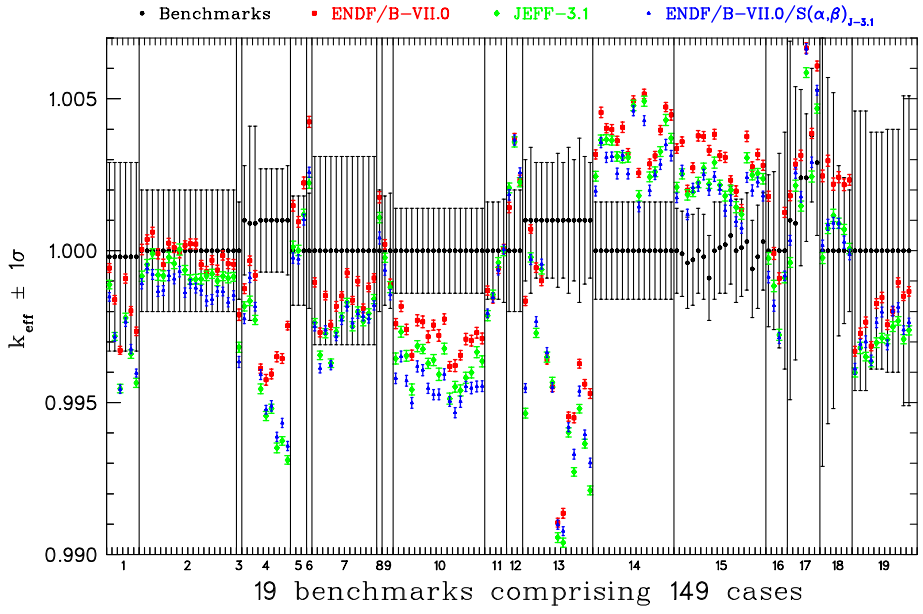

Fig. 2. Calculated and benchmark k_{eff} values with error bars representing one standard deviation.

Table 1
Assignment of the numbers given on the *x*-axis of Figs. 2 and 3 to the corresponding benchmark cases.

Number	Sequence of benchmark cases (increasing)
1	LCT-01-01
	LCT-01-03
	LCT-01-05/LCT-01-08
2	LCT-06-01/LCT-06-18
3	LCT-07-01
4	LCT-11-01/LCT-11-03
	LCT-11-10/LCT-11-15
5	LCT-13-02/LCT-13-04
6	LCT-14-01
7	LCT-16-01/LCT-16-05
	LCT-16-08/LCT-16-14
8	LCT-18-01
9	LCT-35-01
	LCT-35-02
10	LCT-39-01/LCT-39-17
11	LCT-42-01/LCT-42-04
12	LCT-47-01/LCT-47-03
13	LCT-51-01
	LCT-51-02
	LCT-51-09/LCT-01-19
14	LCT-62-01/LCT-62-15
15	LCT-65-01/LCT-65-17
16	MCT-01-01/MCT-01-04
17	MCT-02-01/MCT-02-06
18	MCT-03-01/MCT-03-06
19	MCT-04-01/MCT-04-11

eigenvalue. Many of the k_{eff}^{calc} (ENDF/B-VII.0/$S(\alpha,\beta)_{\text{J-3.1}}$) lie even lower than those obtained using JEFF-3.1. Comparing the red and blue points one may note, as a general feature, that the size of the differences of the k_{eff}^{calc} due to the change of $S(\alpha,\beta)$ varies over a relatively wide range.

In order to highlight the impact of the change of $S(\alpha,\beta)$ on the calculated eigenvalues the differences $\Delta k_1 = k_{eff}^{calc}$ (ENDF/B-VII.0) $- k_{eff}^{calc}$(JEFF-3.1) and $\Delta k_2 = k_{eff}^{calc}$(ENDF/B-VII.0) $- k_{eff}^{calc}$(ENDF/B-VII.0/$S(\alpha,\beta)_{\text{J-3.1}}$) are shown as open circles and filled squares, respectively, in Fig. 3 in units of per cent mile (pcm = 10^{-5}). Quite obviously, the spread of the Δk_2 over a range of approximately −60 to 400 pcm points out that there are benchmarks for which the thermal neutron scattering on hydrogen in water molecules does not play an important role, but there are others for which the impact of $S(\alpha,\beta)$ is quite significant. Furthermore, for many benchmark cases Δk_1 and Δk_2 are found to lie relatively close to each other. Thus the outcome of Fig. 2, that for most of the cases k_{eff}^{calc} (ENDF/B-VII.0) is slightly greater than k_{eff}^{calc} (JEFF-3.1), is, to a significant extent, caused by the different parameterizations for $S(\alpha,\beta)$. For example, the largest difference Δk_1 of the eigenvalues calculated with ENDF/B-VII.0 and JEFF-3.1 is found for case LCT-11-15 and amounts to 442 pcm (the highest open circle in Fig. 3). The difference Δk_2 for LCT-11-15 is 396 pcm (the highest filled square in Fig. 3). Thus for LCT-11-15 just replacing the $S(\alpha,\beta)$ from ENDF/B-VII.0 by that from JEFF-3.1 accounts for ≈90% of the drop in the calculated eigenvalue.

In order to specify the more qualitative results obtained so far, a statistical analysis has been performed in the same manner as described in Kolbe et al. (2008). In the upper part of Table 2, for the sample of normalized eigenvalues $k_{c,i} = k_{eff,i}^{calc} / k_{eff,i}^{bench}$ ($i = 1, \ldots, 149$), the weighted average $\langle k_c \rangle$ and its standard deviation σ', the minima, maxima, and standard deviation s are listed for the suite of 149 benchmark cases calculated with the ENDF/B-VII.0, JEFF-3.1, and ENDF/B-VI.8 cross-section libraries. In the last column of the table also the biases (given by $b = \langle k_c \rangle - 1.0$) resulting from the three cross-section libraries are shown in units of pcm, rounded to multiples of 10. The results of Table 2 confirm that with both ENDF/B-VII.0 and JEFF-3.1 a very good agreement with the benchmark data is reached, leading to very low values of the biases, 10 pcm and 100 pcm, for ENDF/BÙVII.0 and JEFF-3.1, respectively.

In the lower part of Table 2 the impact caused by changes of the thermal neutron scattering cross section for hydrogen in water is shown. The drop of the normalized eigenvalues caused by solely replacing the $S(\alpha,\beta)$ parameterization in ENDF/BÙVII.0 by that in JEFF-3.1, amounts (on the average) to 120 pcm, which is more than the difference of the biases (90 pcm) of ENDF/B-VII.0 and JEFF-3.1. Thus the bias obtained for the ENDF/B-VII.0/$S(\alpha,\beta)_{\text{J-3.1}}$ data (at a value of −130 pcm) even exceeds the value obtained using JEFF-3.1 ($b = -100$ pcm). When the $S(\alpha,\beta)$ for hydrogen in water from ENDF/B-VII.0 is replaced by the corresponding $S(\alpha,\beta)$ from ENDF/BÙVI.8, a similar drop of the normalized eigenvalues is obtained by (on the average) 170 pcm, which is significantly less than the difference of the biases (720 pcm) of ENDF/B-VII.0 and ENDF/BÙVI.8. Finally also the JEFF-3.1 library was applied with the parameterization of $S(\alpha,\beta)$ for hydrogen in water from ENDF/B-VII.0. As expected, it was found that the bias increases now to a value of +10 pcm as shown in the last row of Table 2.

4.2.2. Spectrum for selected benchmark cases

This section aims at a qualitative explanation why the differences $\Delta k_2 = k_{eff}^{calc}$(ENDF/B-VII.0) $- k_{eff}^{calc}$(ENDF/B-VII.0/$S(\alpha,\beta)_{\text{J-3.1}}$) spread over a relatively wide range for all benchmark cases as shown in Fig. 3, i.e., why the impact of a change of $S(\alpha,\beta)$ on the calculated eigenvalues varies from negligible to significant for the benchmark cases of the suite. To this end first LCT-11-15 is looked at, for which, as already mentioned in Section 4.2.1, the difference Δk_2 reaches the maximum of 396 pcm. The key experimental design parameters of all cases of LCT-11 are described in the ICSBEP-handbook (OECD/NEA, 2005). They consist of configurations of individual fuel rods located in arrays, or clusters, with variable space between clusters of rods. In some cases of LCT-11 absorber rods of B_4C were put in the space between the clusters. Particularly for case 15 of LCT-11 the space between the clusters (arranged in a 3 × 3 array) was the largest (of the in total 15 cases that were set up in this benchmark) and was solely filled with ordinary water (no absorbers), as sketched on the left side of Fig. 4. Thus especially the water between the clusters (and to a lesser extent the water reflector of the entire 3 × 3 array) and with it the parameterization of $S(\alpha,\beta)$ had an important impact on the effective multiplication factor of LCT-11-15. The spectrum of the neutron flux calculated with the ENDF/B-VII.0 library in percentage of the total flux is shown by the black line in Fig. 5 for a mesh of 30 energy groups.

Table 2
Results obtained by a statistical analysis of the normalized eigenvalues for a suite of 149 benchmark experiments.

Cross Section Library	$\langle k_c \rangle \pm \sigma'$	Min $k_{c,i} \pm \sigma_i$	Max $k_{c,i} \pm \sigma_i$	Standard deviation s	Bias b [pcm]
ENDF/B-VII.0	0.9999 ± 0.0002	0.9901 ± 0.0022	1.0052 ± 0.0016	0.00303	−10
JEFF-3.1	0.9990 ± 0.0002	0.9894 ± 0.0019	1.0049 ± 0.0016	0.00325	−100
ENDF/B-VI.8	0.9927 ± 0.0002	0.9844 ± 0.0019	0.9998 ± 0.0020	0.00292	−730
ENDF/B-VII.0/$S(\alpha,\beta)_{\text{J-3.1}}$	0.9987 ± 0.0002	0.9898 ± 0.0019	1.0046 ± 0.0016	0.00311	−130
ENDF/B-VII.0/$S(\alpha,\beta)_{\text{E-VI.8}}$	0.9982 ± 0.0002	0.9893 ± 0.0019	1.0038 ± 0.0016	0.00312	−180
JEFF-3.1/$S(\alpha,\beta)_{\text{E-VII.0}}$	1.0001 ± 0.0002	0.9897 ± 0.0019	1.0058 ± 0.0016	0.00320	+10

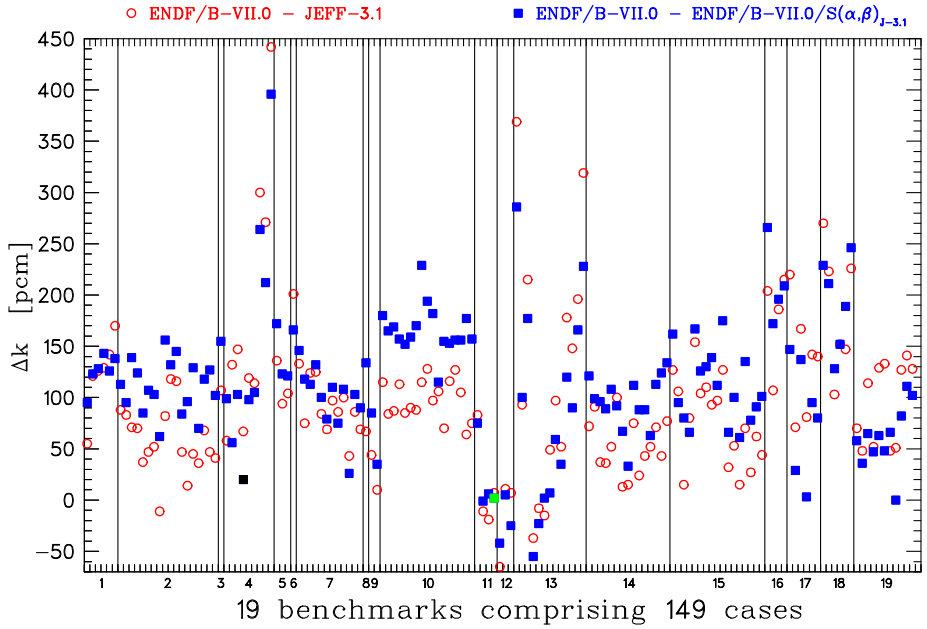

Fig. 3. Differences of the eigenvalues k_{eff}^{calc} determined by applying cross section data based on ENDF/B-VII.0, JEFF-3.1, and ENDF/B-VII.0 with the $S(\alpha, \beta)$ parameterization of JEFF-3.1.

Secondly the setup of LCT-42 was inspected, for which, on the average (over the four cases 01–04 considered in the suite of 149 benchmarks) the impact of $S(\alpha, \beta)$ on the calculated eigenvalues was smallest (just 20 pcm). Particularly for LCT-42-04 the difference Δk_2 amounted to merely 2 pcm (highlighted by the green filled square in Fig. 3). The key experimental design parameters of cases 01–04 of LCT-42 are (from the ICSBEP-handbook (OECD/NEA, 2005)): water-moderated clusters of UO_2 fuel rods separated by steel, boral, or boroflex plates with steel reflecting walls. Especially in configuration LCT-42-04, which is sketched in Fig. 6, the separating plates were made of boroflex which absorbed the thermal neutron flux. Thus the impact of the change of $S(\alpha, \beta)$ on the calculated eigenvalues was very small for this case. The spectrum of the neutron flux, calculated as before, is shown by the red solid line in Fig. 5. In comparison to LCT-11-15 the thermal neutron flux of LCT-42-04 is much smaller.

Another benchmark case not very much affected by $S(\alpha, \beta)$ is LCT-11-10 (Δk_2 = 20 pcm, highlighted by the black filled square in Fig. 3). Contrary to LCT-11-15 the gap between the clusters was very small and filled with B_4C absorber rods (as shown on the right side of Fig. 4), which led to a relatively small thermal neutron flux. The spectrum of the flux is shown in Fig. 5 by the dashed green line.

The cases discussed explain the spread of the differences Δk_2 for the suite of benchmark cases. The impact of the $S(\alpha, \beta)$ parameterization depends to a large extent on the size of the thermal neutron flux. Browsing through the key parameters of all benchmarks further confirms this result. Configurations with a lot of water between or around clusters and no strong absorbers like boron have a high sensitivity to the thermal neutron scattering cross section. Vice versa, configurations with neutron absorbing material between clusters and with reflectors not consisting of water entail a low impact of the $S(\alpha, \beta)$ on the calculated effective multiplication factor.

4.2.3. Comparison of $S(\alpha, \beta)$ cross sections

In Fig. 7 the integral cross sections for inelastic scattering of thermal neutrons on hydrogen in water from the ENDF/B-VII.0, JEFF-3.1, and ENDF/B-VI.8 cross-section libraries are compared. Although there might be differences also in the secondary neutron spectra and angular distributions, these are difficult to compare and analyze. However, it is presumed here that the observed differences

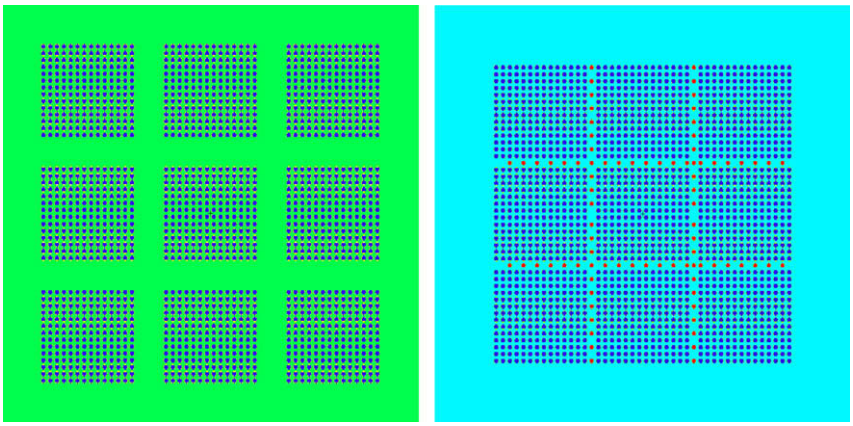

Fig. 4. Configurations of benchmark cases LCT-11-15 (left) and LCT-11-10 (right).

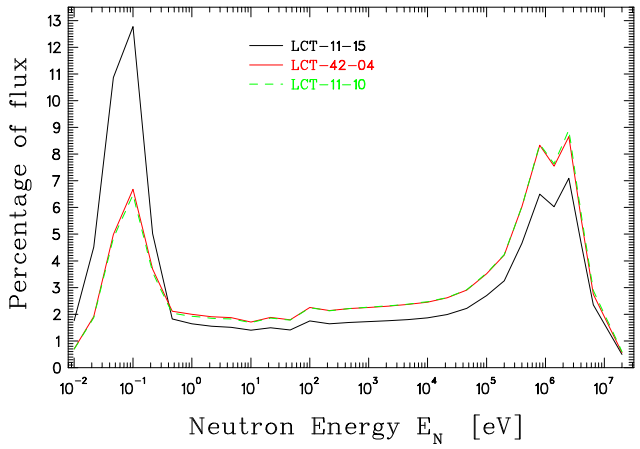

Fig. 5. Neutron flux spectra in the core of selected benchmark cases in 30 energy groups calculated with MCNPX-2.5.0 and the ENDF/B-VII.0 cross section library.

in the integral cross sections may explain the found differences in the calculations with the above specified libraries. The corresponding data were extracted from the files in ACE-format distributed by the sources cited in Section 2.2. Note that the data are also publicly available and can be downloaded from the T-2 Nuclear Information Service at Los Alamos National Laboratory (T-2, 2009). The first striking feature in Fig. 7 is that for neutron energies lower than about 0.001 eV the ENDF/B-VI.8 cross section is significantly larger than those from ENDF/B-VII.0 and JEFF-3.1, which are in close agreement. However, a comparison of the weighted averages $\langle k_c \rangle$ and the biases b obtained with ENDF/B-VII.0, ENDF/B-VII.0/$S(\alpha, \beta)_{\text{J-3.1}}$, and ENDF/B-VII.0/$S(\alpha, \beta)_{\text{E-VI.8}}$ in Table 2 shows, that the $\langle k_c \rangle$ and b calculated with the $S(\alpha, \beta)$ from JEFF-3.1 are closer to the $\langle k_c \rangle$ and b calculated with the $S(\alpha, \beta)$ from ENDF/B-VI.8 than to those calculated with the $S(\alpha, \beta)$ from ENDF/B-VII. Thus the striking difference for neutron energies lower than about 0.001 eV does not have a significant impact on the effective multiplication factors calculated for the suite of benchmarks, due to the fact that the neutron flux for energies lower than 0.001 eV is very small. In the upper right corner of Fig. 7 the cross sections have been zoomed in with a linear scale on the y-axis and in the energy interval from 0.01 eV to 1.0 eV, that is in the range where the neutron fluxes shown in Fig. 5 have peaks. It can be seen that the inelastic thermal scattering cross section from ENDF/B-VII.0 is only slightly smaller than those from JEFF-3.1 and ENDF/B-VI.8 in the energy range 0.01–1.0 eV. Nonetheless it leads to slightly less down-scattering of neutrons in water and thus finally to a larger k_{eff}, as fewer thermal neutrons are absorbed in the water and more thermal neutrons are scattered back into the fuel.

That slightly fewer thermal neutrons are absorbed in the water could be verified by calculating the percentage of neutron captures by isotopes in the core region (according to (OECD/NEA, 2005)) of the benchmark cases LCT-11-15, LCT-11-10, and LCT-42-04 applying the same combinations of cross-section libraries/thermal scattering sublibraries that were already assessed in Table 2. The values of the percentage of neutron captures on hydrogen atoms in water are listed in Table 3 and show that for LCT-11-15, the benchmark case sensitive to the parameterization of $S(\alpha, \beta)$, the percentage of captures on hydrogen noticeably drops when the thermal scattering sublibrary of ENDF/B-VII.0 is applied.

5. Analysis of trends

To get more insight on the effects from the $S(\alpha, \beta)$ updates in the ENDF/B-VII.0 library, an analysis of trends was performed. The impact of the $S(\alpha, \beta)$-parameterization depends to a large extent on the relative fraction of the thermal neutron flux. Therefore, in a first attempt, the normalized eigenvalues $k_{c,i}$ obtained using various combinations of cross-section libraries and parameterizations of $S(\alpha, \beta)$ were plotted as a function of the percentage of the flux in the thermal energy range for all 149 benchmark cases. The analysis for trends consisted of three steps: (1) Weighted linear regression fits to the data were performed with weights proportional to $1/\sigma_i^2$ (where σ_i is the uncertainty of a single observation, see (Kolbe et al., 2008)), and the data and the linear fit were evaluated visually; (2) The slope of the straight line and especially the relative error in the slope were inspected; and (3) The goodness of the linear fit was appraised (following (Press et al., 1992)) by evaluation of the incomplete gamma function Q. Although it was expected to find at least for one of the cross section data sets a weak trend, not any could be found. The data looked like scatter-plots, the slopes of the linear regression fits were small and their relative errors very large. Values for Q less than 0.1% indicated that all fits had to be rejected. However, at second sight, two explanations could be found for the negative outcome of the first trend analysis:

(1) Comparing the total uncertainties σ^{bench} in the benchmark eigenvalues k_{eff}^{bench} with the impact of changing $S(\alpha, \beta)$ one finds that they have the same order of magnitude. The σ^{bench} cover a range of 140–710 pcm (for a confidence level of 1σ),

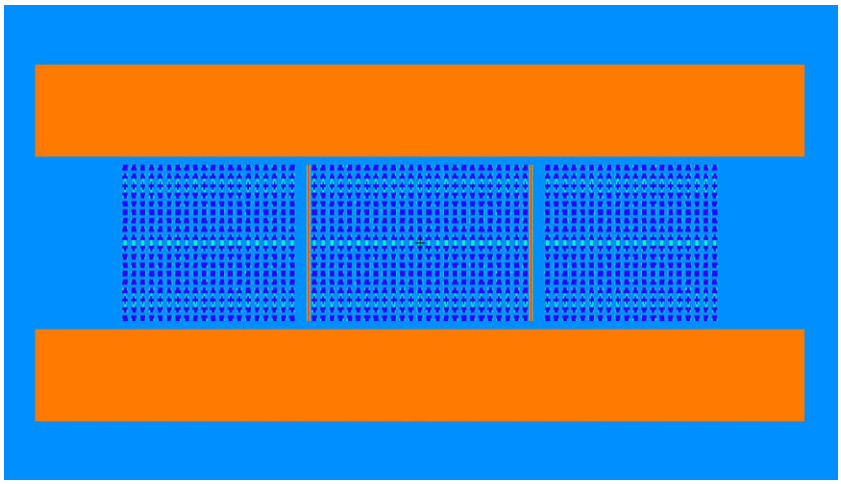

Fig. 6. Configuration of benchmark case LCT-42-04: water-moderated clusters of UO_2 fuel rods separated by boroflex plates with steel reflecting walls.

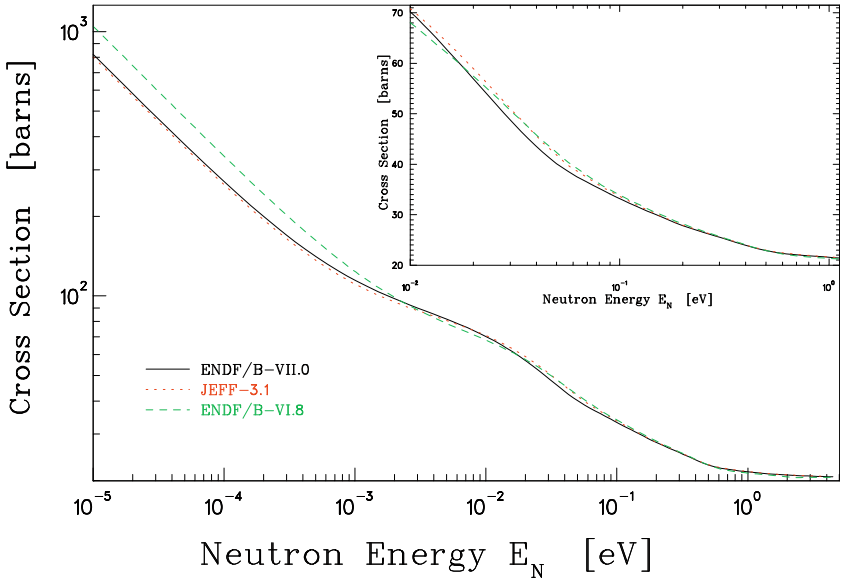

Fig. 7. Cross sections for inelastic thermal neutron scattering on hydrogen in water from the ENDF/BÙVII.0, JEFF-3.1, and ENDF/B-VI.8 cross-section libraries. In the upper right corner the energy interval from 0.01 eV to 1.0 eV is highlighted using a linear scale for the *y*-axis.

Table 3
Comparison of the percentage of neutron captures on hydrogen atoms in water in the core region of the three benchmark cases discussed in Section 4.2.2.

Cross-section library	Benchmark case		
	LCT-11-15 (%)	LCT-11-10 (%)	LCT-42-04 (%)
ENDF/B-VII.0	25.82	8.01	8.31
JEFF-3.1	25.97	8.02	8.31
ENDF/B-VI.8	26.05	7.99	8.29
ENDF/B-VII.0/$S(\alpha,\beta)_{\text{J-3.1}}$	26.02	8.02	8.32
ENDF/B-VII.0/$S(\alpha,\beta)_{\text{E-VI.8}}$	26.06	8.02	8.32
JEFF-3.1/$S(\alpha,\beta)_{\text{E-VII.0}}$	25.78	8.01	8.30

as can be seen in Fig. 2. This makes it very likely that a trend of the normalized eigenvalues $k_{c,i}$ as a function of the flux in the thermal energy range is washed out by a probable (random) scattering of the k_{eff}^{bench} within their errors.

(2) Furthermore, in order to be comparable, the cores of the benchmarks, i.e., the region in which the flux is calculated, should be similar. However, the 149 benchmarks selected from the handbook cover configurations consisting of single arrays of fuel pins as well as several clusters of fuel pins separated by water gaps or absorber plates. While for single arrays the (water) reflector is usually not included in the core, for configurations consisting of several clusters the water (and absorbers) between the clusters is generally included. But a (water) reflector around all clusters does not belong to the core. Thus again it is very likely that an existing weak trend in the $k_{c,i}$ as a function of thermal flux is diluted by the fact that the flux is determined for dissimilar cores.

In order to reduce the so-called "dilution effects" the trend analysis was performed for a subset of cases of the full benchmark suite that belong to similar configurations with similarly defined cores. For this subset all cases (1/3, 10/15) from LCT-11 and all cases (1, 2, 9/19) from LCT-51 were selected, because both experiments involved the same fuel rods located with similar distances between clusters (see OECD/NEA, 2005). While in LCT-11 water and absorber rods where put in the space between clusters, water and absorber plates were used in LCT-51 to isolate different clusters. Furthermore, benchmarks LCT-11 and LCT-51 were performed by the same experimental group. For this subset of 22 cases the systematic errors of the experiments can be expected to be largely the same and thus the scattering of the k_{eff}^{bench} within their uncertainties should be reduced. The σ^{bench} for LCT-11 and LCT-51 cover a range of 170–320 pcm.

A trend analysis for this subset of benchmark cases yielded the results shown in Fig. 8, where the normalized eigenvalues calculated with four combinations of cross-section libraries and $S(\alpha,\beta)$-parameterizations are plotted versus the neutron flux below 4.64 eV. On the top left part of each diagram the slope m obtained for the fit and the absolute error of m are stated. Note that for all regression fits presented in Fig. 8 the evaluation of the incomplete gamma function Q resulted in values $Q \geqslant 10\%$, which indicate good and credible fits.

In the diagram on the top left of Fig. 8 the results calculated with ENDF/B-VII.0 are shown. There is essentially no trend and the slope listed is (within the error) in agreement with zero. Application of JEFF-3.1 clearly leads to a negative trend, as depicted in the diagram on the bottom left of Fig. 8. If the parameterization of $S(\alpha,\beta)$ from ENDF/B-VII.0 is replaced by that of JEFFÙ3.1, the results shown in the diagram on the top right are obtained. Comparing with the plot on the top left it is concluded that the change of the $S(\alpha,\beta)$-parameterization entails a negative trend. Vice versa, applying JEFF-3.1 with the $S(\alpha,\beta)$ from ENDF/B-VII.0, as indicated in the diagram on the bottom right, removes the trend and leads to a negligible slope that is within the error in agreement with zero.

It should be noted that variations of the upper cutoff energy for the neutron flux around the value of 4.64 eV used for the trends analysis, as stated above, did not affect the results shown in Fig. 8. The slopes of the linear regression fits only changed marginally, and the trends as found in Fig. 8 recurred.

It is finally pointed out that replacing the JEFF-3.1 library by the ENDF/B-VI.8 library in Fig. 8 leads to similar results. Clear negative trends occur when the $S(\alpha,\beta)$-parameterization from ENDF/B-VI.8 is applied, and the trends vanish when the $S(\alpha,\beta)$ from ENDF/B-VII.0 is used.

6. Discussion

In Section 4.2.1 it has been found, based on MCNPX-2.5.0 calculations for a suite of 149 benchmarks of type LCT extracted from

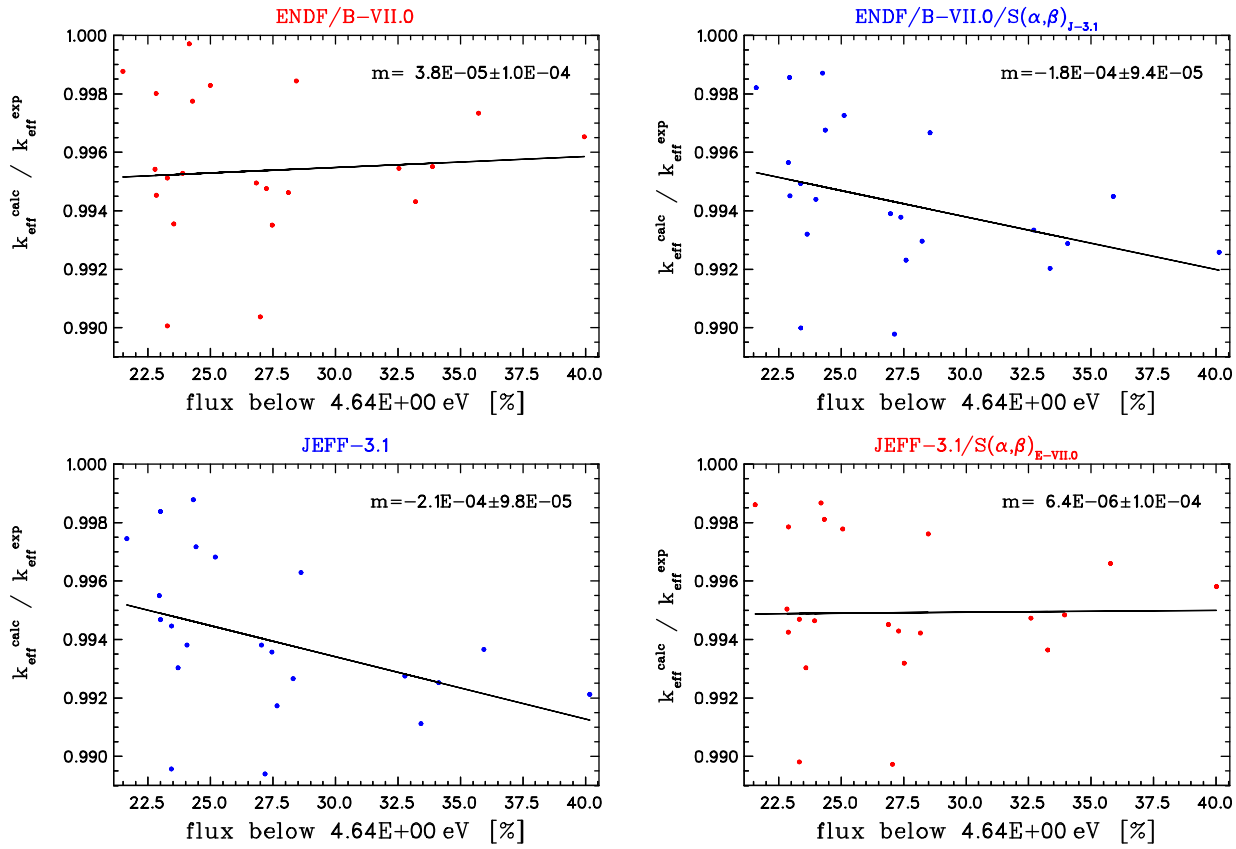

Fig. 8. Results of a trend analysis for a subset of benchmarks. The normalized eigenvalues are plotted versus the neutron flux below 4.64 eV applying four sets of cross section data.

the ICSBEP-handbook, that the impact of differences in the thermal neutron scattering cross sections on the calculated effective multiplication factor k_{eff}^{calc} for the benchmarks varies over a relatively wide range of approximately −60 to 400 pcm. This spread can easily be understood by realizing that the impact of the $S(\alpha, \beta)$-parameterization depends to a large extent on the size of the thermal neutron flux, which can be quite different for different benchmark cases.

By a statistical evaluation of the normalized eigenvalues calculated with the ENDF/B-VII.0 and JEFF-3.1 cross-section libraries biases of 10 pcm and 100 pcm, respectively, were obtained. It turned out that the difference of these biases is largely explained by the different $S(\alpha, \beta)$-parameterizations for hydrogen in water in the libraries, because, solely replacing the $S(\alpha, \beta)$ in ENDF/BÙVII.0 by that in JEFF-3.1, causes a drop of the bias by 120 pcm. Comparing the results obtained using ENDF/BÙVII.0 and ENDF/B-VI.8 in an analogous manner, it is found that the drop of the bias of 170 pcm caused by replacing the $S(\alpha, \beta)$ covers only a smaller fraction of the difference (720 pcm) in the biases calculated for ENDF/BÙVII.0 (10 pcm) and ENDF/BÙVI.8 (730 pcm). The results obtained by replacing the $S(\alpha, \beta)$-parameterization are in nice agreement with the slight increase in the calculated k_{eff} eigenvalues for LCT critical assemblies found in (Chadwick et al., 2006).

A plot of the cross sections for inelastic thermal neutron scattering on hydrogen in water from ENDF/BÙVII.0, JEFF-3.1, and ENDF/B-VI.8 in the relevant energy range shows that the ones for JEFF-3.1 and ENDF/B-VI.8 are quite similar, which also explains that the drops from replacing the $S(\alpha, \beta)$ in ENDF/BÙVII.0 by that in JEFF-3.1 and that in ENDF/B-VI.8 (120 pcm and 170 pcm, respectively) are similar. However, the inelastic thermal neutron scattering cross section of ENDF/B-VII.0 is slightly smaller than the others, resulting from a reevaluation performed for ENDF/B-VII.0 (Chadwick et al., 2006). The question, whether this reevaluation really leads to an improvement of the cross sections, arose, and was tried to answer by a trend analysis of the normalized eigenvalues with respect to percentage of the thermal neutron flux. It turned out that negative trends emerging when using JEFF-3.1 and ENDF/B-VI.8 in the calculations vanished when ENDF/BÙVII.0 was applied or just the $S(\alpha, \beta)$-parameterizations were replaced by the one of ENDF/B-VII.0. These findings indicate that the new thermal neutron scattering kernel for H_2O implemented in ENDF/B-VII.0 seems to mark an improvement.

7. Conclusions

In CSE of wet storage pools it is often necessary to assess several configurations, and, e.g., in addition to the entire storage pool, an analysis of a single FA with a water reflector may be asked for. Even more configurations may have to be included in the simulations, when accident conditions must be considered. Thus in validation activities the suite of benchmarks should contain a range of configurations from single arrays of fuel pins with water reflector to clusters of fuel pins separated by absorbers plates and/or water gaps.

In this paper it has been pointed out that the sensitivity of these configurations to cross sections for thermal neutron scattering in water covers quite a wide range and depends on the size of the thermal neutron flux in the configurations. As the thermal neutron flux of benchmark cases may vary quite a lot, deficiencies in the cross sections for thermal scattering cannot be easily corrected for by establishing and including the bias. Therefore accurate parameterizations of the $S(\alpha, \beta)$ scattering matrix are needed.

By performing trend analyses for a well selected subset of benchmark cases it could be shown that negative trends with respect to the size of the thermal neutron flux, that emerged when using the JEFF-3.1 and ENDF/B-VI.8 cross-section libraries in the calculations, vanished when ENDF/BÙVII.0 was applied. Therefore it is recommended that ENDF/B-VII.0 should be used for CSE of wet storage pools, especially when configurations with a high thermal flux and a water reflector must be assessed.

Finally it is concluded that trend analyses performed within validation activities can be refined by considering well selected subsets of benchmark cases in addition to performing them for the full suite of benchmarks. This may especially be required to discover relatively weak trends.

Acknowledgement

This work has been partially supported by swiss *nuclear*, the organization of the Swiss nuclear utilities.

References

Chadwick, M.B. et al., 2006. ENDF/B-VII.0: next generation evaluated nuclear data library for nuclear science and technology. Nuclear Data Sheets 107, 2931–3060.

Dean, J.C., Tayloe, R.W., Morey, D., 2001. Guide for Validation of Nuclear Criticality Safety Calculational Methodology. NUREG/CR-6698.

Kolbe, E., Vasiliev, A., Ferroukhi, H., Zimmermann, M.A., 2008. Consistent evaluation of modern nuclear data libraries for criticality safety analyses of thermal compound low-enriched-uranium systems. Annals of Nuclear Energy 35, 1831–1841.

MacFarlane, R.E., 1994. New Thermal Neutron Scattering Files for ENDF/B-VI, Release 2. Technical Report LA-12639-MS (ENDF 356), Los Alamos National Laboratory.

MacFarlane, R.E., Muir, D.W., 1994. The NJOY Nuclear Data Processing System. Version 91. Technical Report LA-12740-M, Los Alamos National Laboratory.

Mattes, M., Keinert, J., 2005. Thermal Neutron Scattering Data for the Moderator Materials H_2O, D_2O, and ZrH_x in ENDF-6 Format and as ACE Library for MCNP(X) Codes. Report INDC(NDS)-0470, IAEA.

MCNP, 2009. <http://mcnp-green.lanl.gov/>.

MCNPX, 2009. <http://mcnpx.lanl.gov/>.

OECD/NEA Data Bank, 2004. ZZ-MCB-ENDF/B-6.8, MCB Continuous-Energy Neutron Cross Section Libraries for Temperatures from 300 to 1800 K, OECD/NEA Data Bank, Paris, France. <http://www.nea.fr/abs/html/nea-1669.html>.

OECD/NEA Data Bank, 2005. International Handbook of Evaluated Criticality Safety Benchmark Experiments, OECD/NEA Data Bank, Paris, France. <http://www.nea.fr/abs/html/nea-1486.html>.

OECD/NEA Data Bank, 2006. ZZ-MCJEFF3.1NEA, MCNP Neutron Cross Section Library based on JEFF3.1, OECD/NEA Data Bank, Paris, France. <http://www.nea.fr/abs/html/nea-1768.html>.

Parks, D.E., Nelkin, M.S., Beyster, J.R., Wikner, N.F., 1970. Slow Neutron Scattering and Thermalization. W.A. Benjamin, Inc., New York.

Pelowitz, D.B., (Ed.), 2005. MCNPX User's Manual, Version 2.5.0. Technical Report LA-CP-05-0369, Los Alamos National Laboratory.

Press, W.H., Teukolsky, S.A., Vetterling, W.T., Flannery, B.P., 1992. Numerical Recipes in FORTRAN: the Art of Scientific Computing, second ed. Cambridge University Press.

RSICC, 2007. ENDF/B-VII.0 in ACE-Format. Radiation Safety Information Computational Center, Package ID: D00226MNYCP01, Oak Ridge National Laboratory, Oak Ridge, USA.

Squires, G.L., 1996. Thermal Neutron Scattering. Dover Publications, Inc., Mineola, New York.

T-2, 2009. T-2 Nuclear Information Service, run by Group T-16 (Nuclear Physics) of the Theoretical Division of the Los Alamos National Laboratory. <http://t2.lanl.gov/data/data.html>.

Vasiliev, A.V., Lebenhaft, J.R., Zimmermann, M.A., 2005. Analysis of MCNPX/JEF-2.2 and JENDL-3.3 Results for a Suite of Low-Enriched Thermal Compound Uranium Benchmarks. 'M&C-2005' International Topical Meeting, Avignon, France.